Geochemistry Geophysics Geosystems G3
AN ELECTRONIC JOURNAL OF THE EARTH SCIENCES
Published by AGU and the Geochemical Society

Article
Volume 9, Number 7
1 July 2008
Q07001, doi:10.1029/2008GC002019
ISSN: 1525-2027

Revised Pacific-Antarctic plate motions and geophysics of the Menard Fracture Zone

Marcel B. Croon and Steven C. Cande
Scripps Institution of Oceanography, University of California, San Diego, 9500 Gilman Drive, La Jolla, California 92093-0220, USA (mcroon@ucsd.edu)

Joann M. Stock
California Institute of Technology, 1200 East California Boulevard, 252-21, Pasadena, California 91125, USA

[1] A reconnaissance survey of multibeam bathymetry and magnetic anomaly data of the Menard Fracture Zone allows for significant refinement of plate motion history of the South Pacific over the last 44 million years. The right-stepping Menard Fracture Zone developed at the northern end of the Pacific-Antarctic Ridge within a propagating rift system that generated the Hudson microplate and formed the conjugate Henry and Hudson Troughs as a response to a major plate reorganization ~45 million years ago. Two splays, originally about 30 to 35 km apart, narrowed gradually to a corridor of 5 to 10 km width, while lineation azimuths experienced an 8° counterclockwise reorientation owing to changes in spreading direction between chrons C13o and C6C (33 to 24 million years ago). We use the improved Pacific-Antarctic plate motions to analyze the development of the southwest end of the Pacific-Antarctic Ridge. Owing to a 45° counterclockwise reorientation between chrons C27 and C20 (61 to 44 million years ago) this section of the ridge became a long transform fault connected to the Macquarie Triple Junction. Following a clockwise change starting around chron C13o (33 million years ago), the transform fault opened. A counterclockwise change starting around chron C10y (28 millions years ago) again led to a long transform fault between chrons C6C and C5y (24 to 10 million years ago). A second period of clockwise reorientation starting around chron C5y (10 million years ago) put the transform fault into extension, forming an array of 15 en echelon transform faults and short linking spreading centers.

Components: 7980 words, 12 figures, 1 table.

Keywords: Pacific-Antarctic Ridge; Menard Fracture Zone; relative motions; uncertainties; tectonics; magnetic anomalies.

Index Terms: 3040 Marine Geology and Geophysics: Plate tectonics (8150, 8155, 8157, 8158).

Received 5 March 2008; **Revised** 5 May 2008; **Accepted** 15 May 2008; **Published** 1 July 2008.

Croon, M. B., S. C. Cande, and J. M. Stock (2008), Revised Pacific-Antarctic plate motions and geophysics of the Menard Fracture Zone, *Geochem. Geophys. Geosyst.*, *9*, Q07001, doi:10.1029/2008GC002019.

1. Introduction

[2] The Pacific-Antarctic Ridge (PAR) (Figure 1) is one of the major branches in the global ridge system and links the Pacific basins to the Earth's other tectonic plates [*Pitman et al.*, 1968]. *Molnar et al.* [1975] first estimated rotation parameters for the PAR, calculating rotations for six chrons, the oldest being C31 (68 Ma [*Cande and Kent*, 1995]), as well as a fit of the Campbell Plateau and Marie Byrd Land. *Cande et al.* [1995] significantly im-

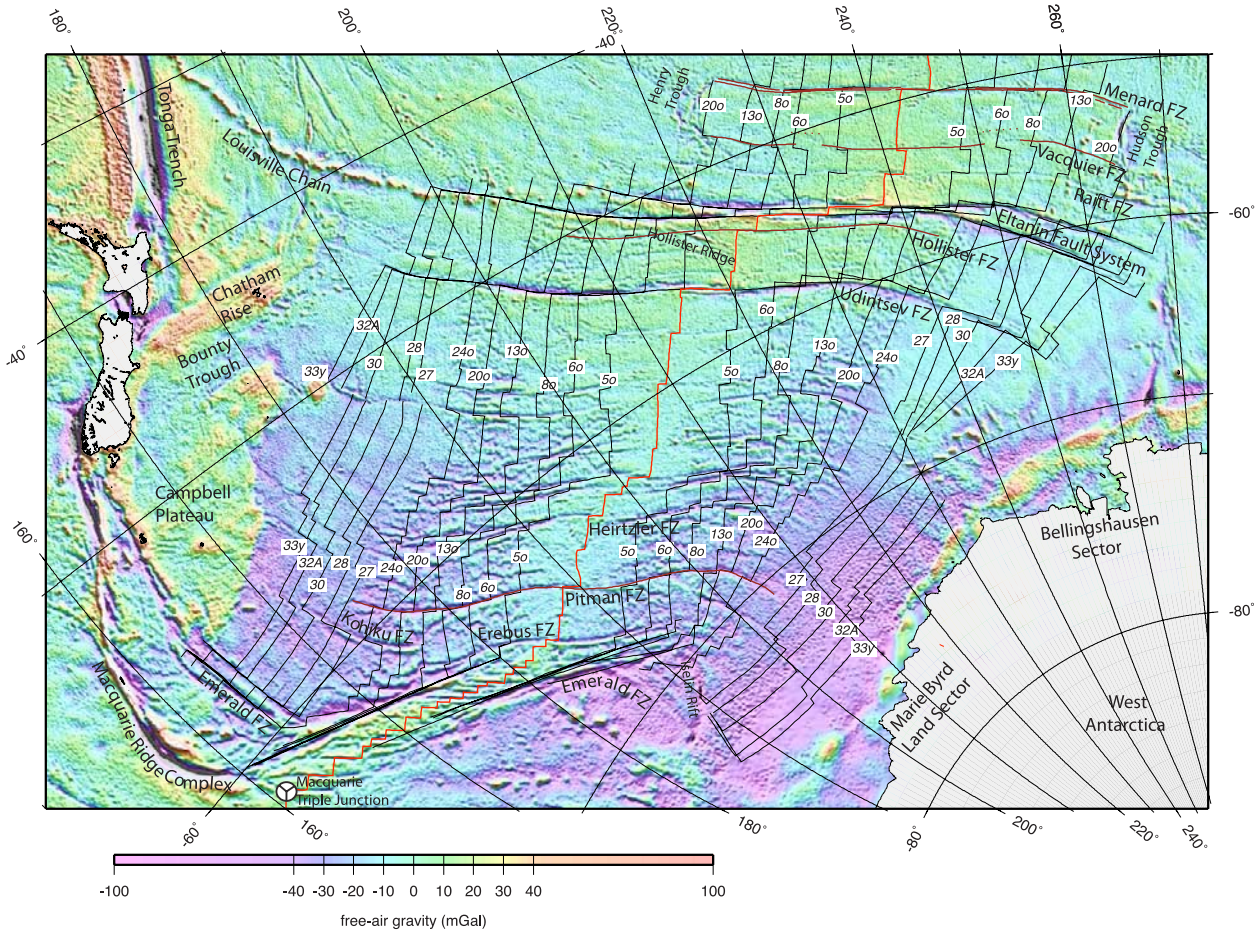

Figure 1. Map of the Pacific-Antarctic Ridge, on an image of the satellite-derived, free-air gravity field, summarizing the location of magnetic anomaly isochrons. The traces of the Menard, Vacquier, Hollister, and Pitman FZs are highlighted in red. Map is in an oblique Mercator projection about a pole at 66.8°N, 81.7°W, near the pole of rotation of Pacific to Antarctica at chron C3A.

proved constraints for Pacific-Antarctic plate motions back to chron C31 (68 Ma) on the basis of data from a detailed geophysical survey of the Pitman Fracture Zone (FZ). In this paper we present a refinement of Pacific-Antarctic plate rotations since ~44 Ma based primarily on new shipboard magnetic anomaly and multibeam bathymetry data along the right-stepping Menard FZ, which developed at the northern side of the PAR within a propagating rift system that generated the conjugate Henry and Hudson Troughs as a response to a major plate reorganization around chron C21 (~45 Ma) [*Cande et al.*, 1982; *Eakins*, 2002].

[3] On the basis of the new magnetic anomaly and FZ data we calculated 49 new rotations for chrons C20o to C1o (43.8 to 0.78 Ma). This allowed us to analyze changes in plate motion along the PAR in detail during this time period. In this paper we present detailed bathymetric and magnetic anomaly data along the Menard FZ, which shows the response of the FZ to adjustments in plate motion. Changes in spreading direction at chrons C13o and C6C (33.5 and 24.1 Ma) are observed at FZs along the entire PAR. We then use these rotations to investigate the tectonic evolution of the southwesternmost section of the PAR, a region which underwent a significant clockwise change in spreading direction during the Late Miocene [*Cande et al.*, 1995; *Lodolo and Coren*, 1997]. Being close to the rotation poles, this area is ideal for testing the predictive quality of the new rotation parameters for changes in plate motion and observed tectonic features related to these changes. We show that a clockwise change in plate motion starting around

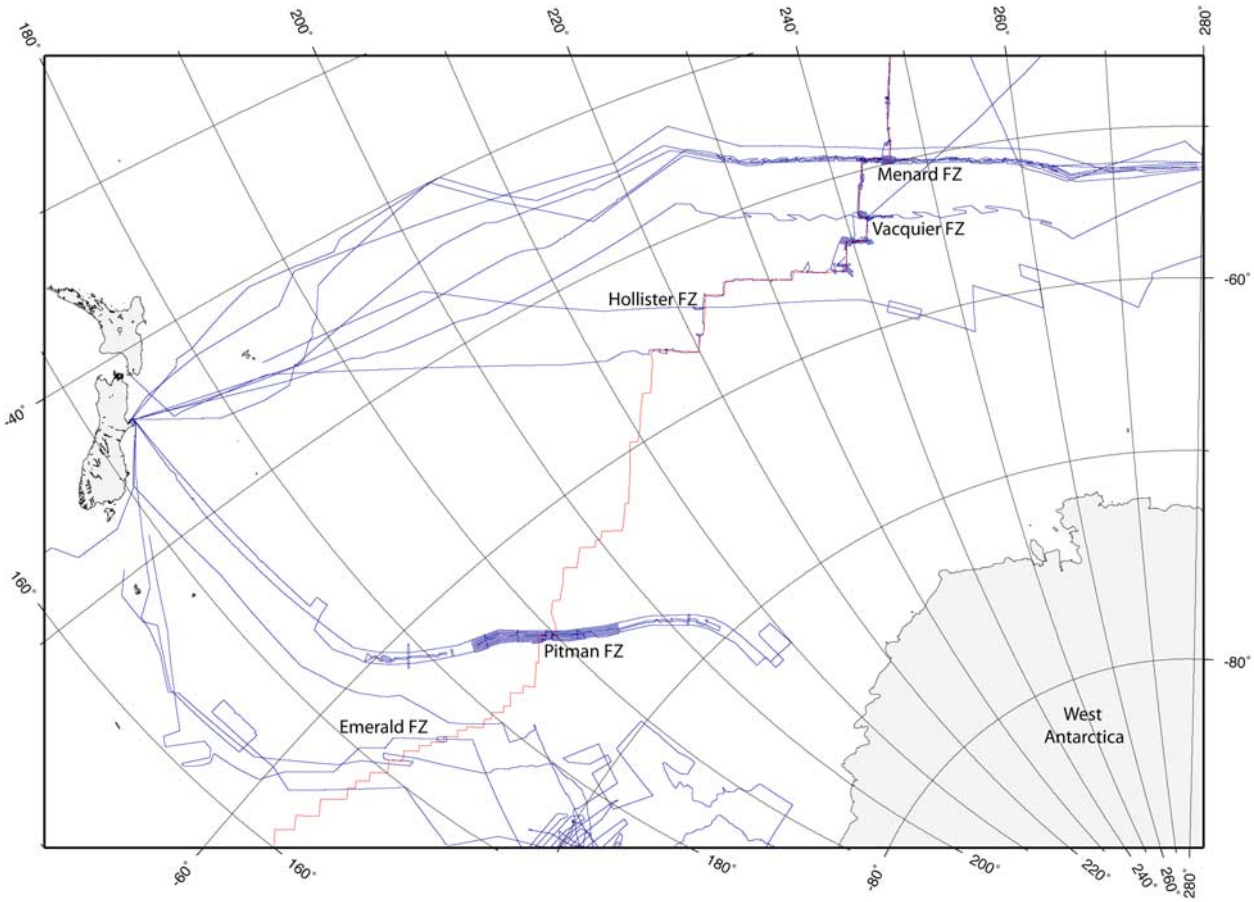

Figure 2. Overview of ship tracks (blue lines) with geophysical data used to improve Pacific-Antarctic rotation parameters. Included are the following cruises (NBP, R/VIB *Nathaniel B. Palmer*; MV, R/V Melville; WT, R/V *Thomas Washington*; RC, R/V *Robert D. Conrad*; EW, R/V *Maurice Ewing*): NBP9707, NBP0007B, NBP0403, NBP0501B, NBP0507, WEST03MV, RAPA03WT, and RC1714 at Menard FZ, NBP0607A at Vacquier FZ, NBP9804 south of Hollister FZ, EW9201 at Pitman FZ, and NBP9702, NBP0209, NBP0501A, and NBP0701 near Emerald FZ. The present location of the Pacific-Antarctic Ridge is highlighted in red. Map projection same as in Figure 1.

chron C5y (9.7 Ma) opened up an array of 15 en echelon transform faults and 15 short linking spreading centers.

2. Data

[4] The most recent major revision to Pacific-Antarctic rotation parameters [*Cande et al.*, 1995] was based on P-code GPS-navigated R/V *Maurice Ewing* data for the Pitman FZ plus older geomagnetic data from available cruises where navigation was less precise. For this study we used the R/V *Maurice Ewing* data plus new data from 11 transits of the NSF OPP (Office of Polar Programs) operated R/VIB *Nathaniel B. Palmer* that are all GPS-navigated and include multibeam bathymetry. These data are mainly concentrated along the Menard FZ and were collected during five R/VIB *Nathaniel B. Palmer* transits between Lyttelton, New Zealand and Punta Arenas, Chile from 1997 to 2005. In addition we used R/VIB *Nathaniel B. Palmer* data from eight transits at the southwest end of the PAR (from 1995 to 2007), one transit along the Vacquier FZ (2006) and one transit south of the Hollister FZ (1998). *Cande and Stock* [2004a, 2004b] calculated Pacific-Antarctic rotations for a small set of chrons using data from a limited number of R/VIB *Nathaniel B. Palmer* transits available at that time. Those rotations are not as well constrained as the rotations presented here. Figure 2 shows ship tracks of all cruises we used for this study. We also used GEOSAT and ERS 1 gravity anomaly data derived from satellite altimetry [*Sandwell and Smith*, 1997; *McAdoo and Laxon*, 1997], for interpretation of tectonic features where magnetic anomaly and bathymetric data were sparse or unavailable.

[5] The principal new data set from the Menard FZ mapped seafloor of the Pacific and Antarctic plates back to its original appearance at ~45 Ma between chrons C20o and C21y (43.8 to 46.3 Ma). Besides the R/VIB *Nathaniel B. Palmer* data we included multibeam bathymetry data from a R/V *Thomas Washington* along-axis survey of the northern section of the PAR [*Lonsdale*, 1994a], a N/O *Atalante* cruise in 2005 [*Klingelhoefer et al.*, 2006] at the Menard transform fault and a R/V *Melville* cruise in 1994 [*Lonsdale*, 1994b] that crossed the Menard FZ on Antarctic plate crust formed around chron C5. The only transit satellite navigated data used in the solutions were from a R/V *Robert D. Conrad* cruise in 1974 that ran south of the Menard FZ on the Antarctic plate between chrons C12o and C20o (30.9 to 43.8 Ma). These data agree well with a parallel GPS-navigated R/VIB *Nathaniel B. Palmer* track. The magnetic anomaly data and identified anomaly points are shown on Figure 3, which is an overview of both the Pacific and Antarctic limbs of the FZ on a GEOSAT gravity background. Detailed multibeam bathymetry (Figures 4a–4e) reveals several prominent features along the Menard FZ including a deep transform fault graben, a westward ridge jump south of the FZ around chron C7 (24.8 Ma) and the presence of two splays, 30 km apart at chron C20o (43.8 Ma), that narrowed to a 5 to 10 km corridor by chron C6C (23.8 Ma).

[6] The other area with considerable new data is at the southwest end of the PAR. In this region a change in spreading direction around chron C5y (9.8 Ma) put a large transform fault under extension, forming a set of short ridge segments. The FZs and several prominent tectonic features are imaged in GEOSAT gravity [*Sandwell and Smith*, 1997] (Figure 5a). The FZ traces are based on the sparse multibeam bathymetry and GEOSAT gravity data (Figures 5b and 5c). Pronounced axial grabens are observed for the ridge segments between FZ E, the Emerald FZ and FZ F, whereas smooth triangular morphology with an axial high [*Macdonald et al.*, 1988] is observed for ridge segments between FZs C and D, FZs H and I and FZs K and L. Troughs of 5000 to 6000 m depth and parallel ridges that reach up to about 1000 m below sealevel mark the boundaries of the en echelon right-stepping FZs.

[7] The preservation of both flanks of the Pacific-Antarctic spreading center allows us to match FZ trails on each flank with the other and compare them with modeled synthetic flow lines [*Cande et al.*, 1988, 1995]. The FZs were digitized from the detailed topography in combination with magnetic anomaly data. We used the geophysical data collected along Menard, Vacquier, Hollister, Pitman, Emerald, C, D, F, H, I and J FZs to calculate a revised set of rotation parameters. A combination of detailed topography, magnetics and minima in GEOSAT gravity data was used to maximize coverage. A total of 49 rotations describe the relative plate motion. Since the Menard FZ, along which most new data were collected, opened at about 45 Ma the oldest improved rotation parameter is chron C20o (43.8 Ma). We identified the magnetic anomalies according to the scheme for the North Pacific initiated by *Atwater and Severinghaus* [1989].

3. Finite Rotations

[8] The finite rotations (Table 1) were calculated using the fitting criteria of *Hellinger* [1981] as implemented by *Chang* [1987, 1988] and *Royer and Chang* [1991]. In this method, reconstruction parameters are determined by dividing the data into multiple segments and fitting great circles to reconstructed data in each segment. Magnetic anomalies and FZ crossings define the segments. On the basis of the multibeam bathymetry we digitized the FZs and also the abyssal hills where magnetic anomaly data were sparse. Table 1 shows the number of segments used for each individual finite rotation. We assigned an average uncertainty estimate of 0.7 to 1.2 km for magnetic anomaly picks, which mainly reflects the ambiguities in identifying specific points on the magnetic anomaly profiles. For FZ crossings a larger 1.7 to 3 km estimate was assigned since the structure of a FZ depends on the geologic history of the transform fault and may change with time [*Lonsdale*, 1994b]. For certain segments only a single track of magnetic anomaly data was available. For these segments abyssal hill morphology was used to extrapolate the magnetic anomaly pick to the outer edges of the multibeam swath generating two extra picks at that location. A 1.7 to 3 km uncertainty was assigned for these picks. Using the *Chang* [1987, 1988] method, a statistical parameter $\hat{\kappa}$ is returned with the solution. $\hat{\kappa}$ is a statistical parameter related to the error values; errors are overestimated when $\hat{\kappa} \gg 1$, errors are underestimated when $\hat{\kappa} \ll 1$. The $\hat{\kappa}$ values we present range between 1 and 3 indicating our error values were somewhat overestimated.

[9] In Figure 6 we compare the newly calculated finite rotation poles with those of *Cande et al.* [1995]. Owing to the large number of constraints

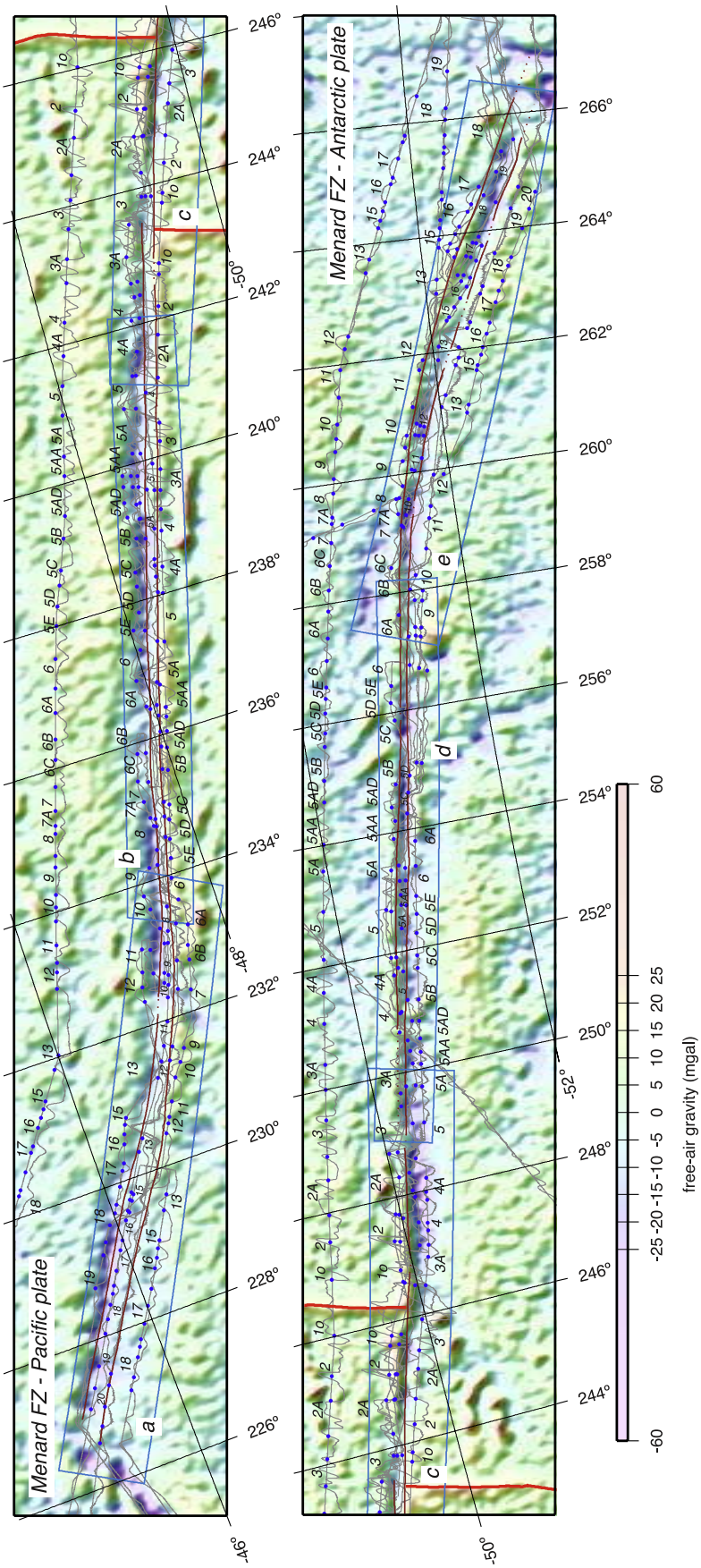

Figure 3. The ship tracks (NBP9707, NBP0007B, NBP0403, NBP0501B, NBP0507, WEST03MV, RAPA03WT, and RC1714) and magnetic anomaly wiggles (gray) along the two splays of the Menard FZ (dark red lines), on an image of the satellite-derived, free-air gravity field. The blue dots represent magnetic anomaly picks, and the Pacific-Antarctic Ridge is highlighted with thick red lines. The blue boxes show the locations of the multibeam bathymetry maps in Figure 4. Map projection same as in Figures 1 and 2.

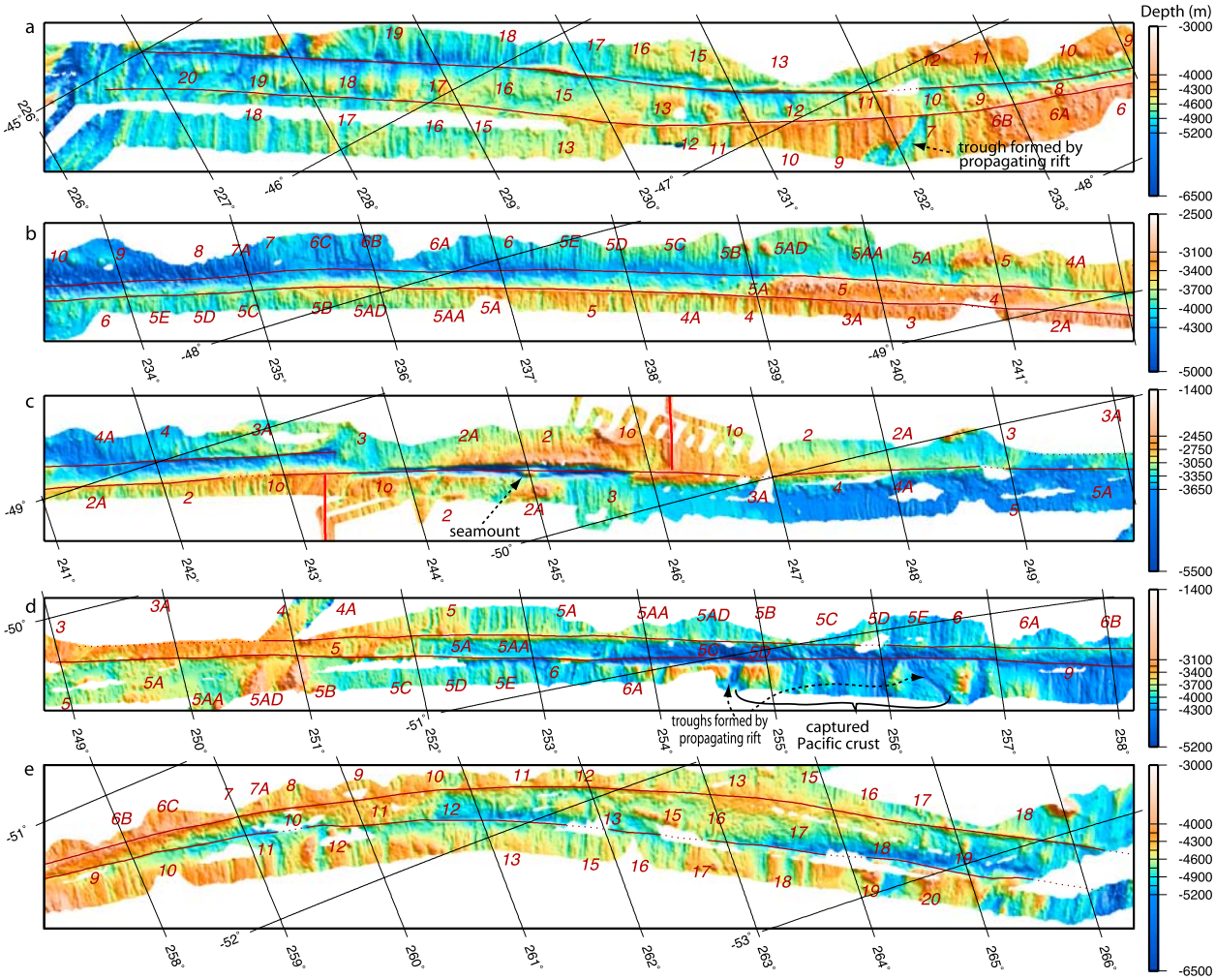

Figure 4. Multibeam bathymetry data from NBP9707, NBP0007B, NBP0403, NBP0501B, NBP0507, WEST03MV, Pacantarctic2, and RAPA03WT cruises at the two splays of the Menard FZ (dark red lines). The red numbers show magnetic anomaly identifications, and the Pacific-Antarctic Ridge is highlighted with thick red lines.

on rotation parameters along the PAR, the error ellipses are very small. Our rotations generally agree well with those of *Cande et al.* [1995], but deviate considerably for times younger than chron C5A (12.3 Ma). This reflects the fact that the trace of the Menard FZ was not well constrained without multibeam bathymetry data. The differences are illustrated (Figure 6) by the 95% error ellipses for chron C5A and younger from *Cande et al.* [1995]. Rotation parameters between chrons C13o and C20o (33.5 to 43.8 Ma) were not constrained in the *Cande et al.* [1995] study. However the pole positions for chrons C13o and C20o are close to our new rotation poles.

[10] The high density of shipboard magnetic anomaly and multibeam bathymetry data on the Menard and Pitman FZs allowed us to address an issue related to intraplate deformation. In particular, *Géli et al.* [1998] suggested that the Hollister Ridge, a prominent volcanic lineament that cuts through 0.5 to 20 Ma old crust near the Hollister FZ (Figure 1), may have been caused by a period of intraplate deformation starting around 3 Ma. We followed the method of *Goodwillie and Parsons* [1992] and *Gans et al.* [2003] and used a comparison of the separation distances between the Menard and Pitman FZs on conjugate portions of the Pacific and Antarctic plates to place an upper limit on the amount of intraplate deformation that may have taken place. The geometrical setup of the *Chang* [1987, 1988] method is ideal for this analysis since the computation for each segment includes the distance between each data point and a great circle

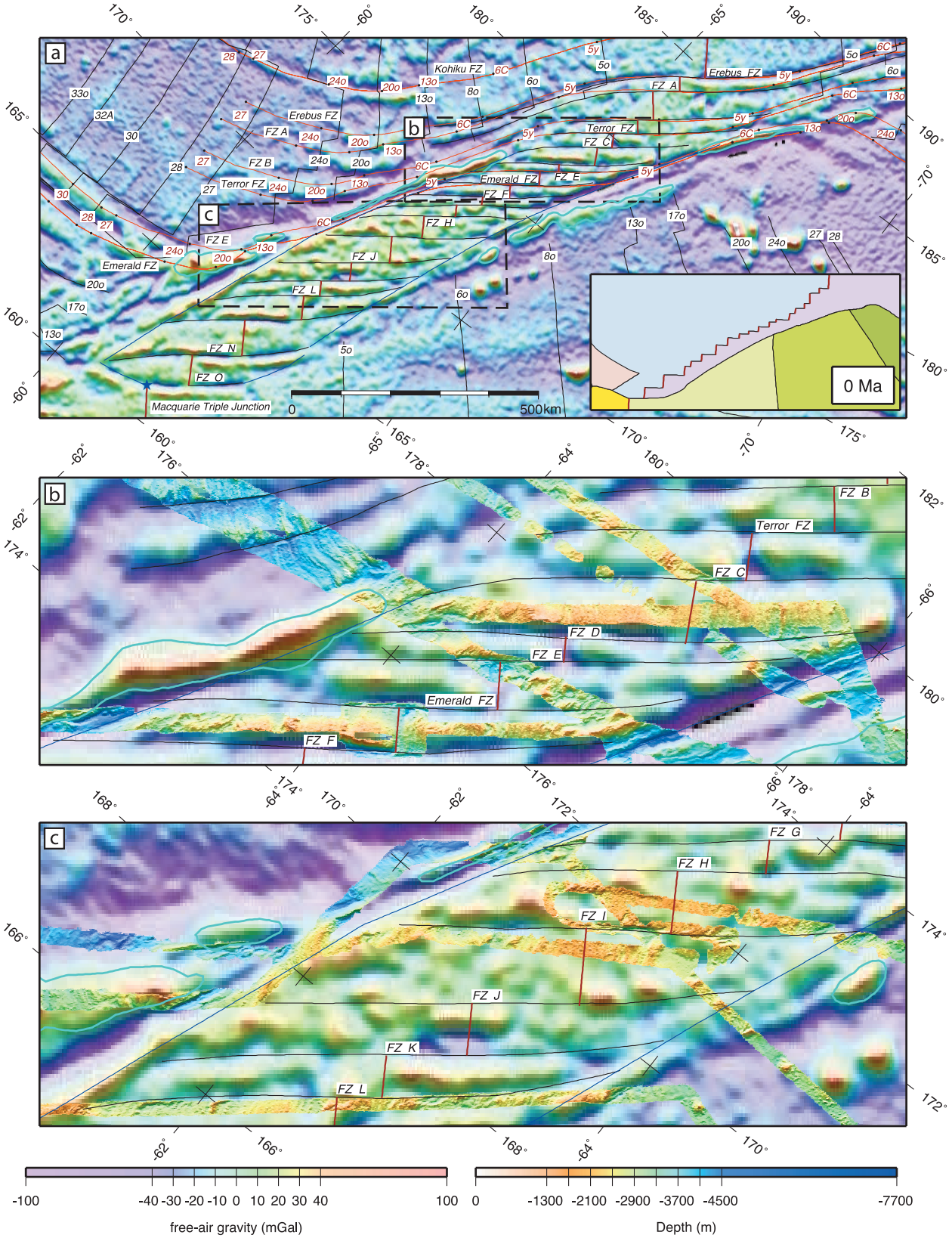
a
b
c
Kohiku FZ
Erebus FZ
Terror FZ
Emerald FZ
FZ A
FZ B
FZ C
FZ D
FZ E
FZ F
FZ G
FZ H
FZ I
FZ J
FZ K
FZ L
FZ N
FZ O
Macquarie Triple Junction
0
500km
0 Ma
-100 -40 -30 -20 -10 0 10 20 30 40 100
free-air gravity (mGal)
0 -1300 -2100 -2900 -3700 -4500 -7700
Depth (m)

Figure 5

that best fits the data in the segment. Thus, the combined misfit of the great circle segments corresponding to the Menard and Pitman FZs is a direct computation of the difference in separation distances between the FZs, which are roughly 3500 km apart. Intraplate deformation should appear as a systematic change in the average amount of misfit between the FZs. When we plot the individual and combined misfits in the FZ segments for all 49 rotations (Figure 7), we noted that the combined misfits are generally about 1.5 km, with no obvious trend to the misfits through time. Although it is difficult to estimate the amount of systematic error in picking the FZ location from the bathymetry because of such tectonic complexities as overshot ridges at ridge-transform intersections [*Gallo et al.*, 1986; *Lonsdale*, 1994b], the lack of any trend to the combined misfit between Menard and Pitman FZs over 45 Ma suggests that the systematic error is small and that any intraplate deformation is less than 1.5 km. The lack of any trend to the misfit also places a lower limit on plate rigidity. A strain of 1.5 km over a distance of 3500 km over 45 Ma corresponds to a strain rate of 9.5×10^{-12}/a, which is within the range suggested for the interior of rigid plates by *Gordon* [1998].

4. Stage Rotations

[11] To evaluate the predictive quality of the new finite rotations we calculated stage rotations and used these to generate synthetic flow lines (Figure 8). These tracks plotted relative to the Pacific and Antarctic plates indicate slow to intermediate spreading rates close to the stage poles (Emerald and Pitman FZs) to intermediate spreading rates further away from the stage poles (Menard and Hollister FZs). Between chrons C20o and C16y (43.8 to 35.7 Ma) the stage poles moved eastward. They experienced a rapid shift westward away from the ridge between chrons C16y and C10y (35.7 to 28.3 Ma). From chrons C8o to C6C (26.6 to 23.1 Ma) the stage poles rapidly moved southeast. Between chrons C6o and C5A (20.1 to 12.3 Ma) they remained relatively stationary. Since chron C5A (12.3 Ma) the stage poles have migrated relatively continuously north-northwest, with a slight change in direction to the north since chron C5y (9.7 Ma). Figure 8 also shows the calculated synthetic flow lines from the stage poles for several FZs along the PAR. The synthetic flow line data fit well with the Menard, Hollister and Pitman FZs. Only the left-stepping Vacquier FZ does not follow a simple synthetic flow line. However, propagating rifts complicated the evolution of the Vacquier FZ between chrons C6C (22.2 Ma) and C5A (12.3 Ma).

5. Variations in Spreading Rates

[12] Using new rotation parameters, we examined the half-spreading rates along the PAR since the opening of the Menard FZ at about 45 Ma. We determined the half-spreading rates for ridge segments bounding the Menard, Hollister, Pitman and Emerald FZs along synthetic flow lines, using the *Cande and Kent* [1995] (CK95) geomagnetic polarity timescale with revisions for chrons C3Ay and C3Ao as given by *Krijgsman et al.* [1999] (Figure 9). The intermediate spreading rate of the PAR at the latitude of the Menard FZ is comparable to the northern part of the Pacific-Cocos [*Weiland and Macdonald*, 1996] and Australian-East Antarctic [*Cochran and Sempéré*, 1997] boundaries. From chrons C20o to C17y (43.8 to 36.6 Ma) the half-spreading rate was fairly constant at about 27 mm/a. Between chrons C17y and C12o (36.6 to 30.9 Ma) the half-spreading rate gradually increased to 40 mm/a. At chron C9o (28.0 Ma) it dropped to 33 mm/a and remained constant until chron C6C (24.1 Ma). Between chrons C6C and C5Cy (24.1 to 16.2 Ma) half-spreading rates were 28 mm/a. *DeMets et al.* [1990] and *Lonsdale* [1994a] reported symmetric spreading at an average half-spreading rate of 47 mm/a since chron

Figure 5. Emerald, Terror, and Erebus FZs and FZs A through O (black lines) on an image of the satellite-derived, free-air gravity field. The black tagged lines are isochrons based on magnetic anomaly picks, and the Pacific-Antarctic Ridge is highlighted with thick red lines. Red tagged lines are synthetic flow lines generated from the stage rotations; blue dots mark the center points of the flow lines. Blue lines mark the edges of the array of FZs A through O, and the bounding transverse ridges are contoured light blue. Inset in Figure 5a: map of seafloor spreading provinces. The blue and purple regions were generated by Pacific-Antarctic spreading, the yellow and light green regions were generated by Australia-East Antarctic spreading, the green region was generated by Australia-Antarctic spreading before chron C8 (26.6 Ma), the dark green region was generated by Australia-Lord Howe Rise (Tasman Sea) spreading, and the pink region was generated by Australia-Pacific spreading between chrons C20 and C8 (43.8 to 26.6 Ma). Detailed maps in Figures 5b and 5c show the available multibeam bathymetry data from NBP9407, NBP9702, NBP9909, NBP0209, NBP0305A, NBP0402, NBP0501A, and NBP0701 cruises on an image of the satellite-derived, free-air gravity field. Map projection same as in Figures 1, 2, and 3.

Table 1. Finite Rotations and Covariance Matrices of the Pacific Plate Relative to the Antarctic Plate[a]

Age (Ma)	Mag. An.	Polarity Chron	Lat. (°N)	Long. (°E)	Angle (deg)	$\hat{\kappa}$	a	b	c	d	e	f	g	Mag. Pts	FZ Pts	Ab. hill Pts	Mag. Segs	FZ Segs
0.78	1o	C1n (o)	64.303	−81.212	0.676	2.62	1.18	.647	1.59	4.26	7.92	4.43	9	43	45	23	9	3
1.86	2	C2n (m)	64.901	−81.138	1.606	1.21	9.05	.251	8.38	6.54	9.72	3.00	9	34	32	14	6	2
2.58	2Ay	C2An.1n (y)	65.204	−81.225	2.227	2.05	27.8	−0.669	2.00	2.37	3.41	8.94	9	32	31	10	5	2
3.58	2Ao	C2An.3n (o)	65.897	−81.165	3.109	1.38	10.4	.661	12.3	8.30	13.1	42.8	9	31	34	15	6	2
4.24	3y	C3n.1n (m)	66.624	−80.533	3.702	2.43	10.0	.662	10.1	7.62	11.4	34.4	9	29	35	8	4	2
5.11	3o	C3n.4n (m)	66.909	−80.658	4.480	2.62	13.6	1.47	19.6	7.24	13.3	58.6	9	30	39	12	5	3
6.04	3Ay	C3An.1n (y)	67.091	−81.081	5.211	2.91	3.53	2.55	4.27	3.23	4.07	8.12	8	28	39	6	4	3
6.71	3Ao	C3An.2n (o)	67.331	−81.202	5.808	1.48	1.32	.240	2.17	.821	1.54	6.55	8	26	41	7	4	3
7.86	4	C4n.2n (m)	68.162	−80.540	6.830	1.41	2.38	.954	4.41	1.50	2.67	11.8	8	30	41	9	5	3
8.86	4A	C4An (m)	68.833	−79.969	7.639	1.34	1.12	.339	1.69	.968	1.56	5.03	8	29	44	11	5	3
9.74	5y	C5n.1n (y)	69.707	−78.566	8.417	1.01	1.59	597	3.17	1.22	2.32	8.91	8	28	45	9	5	3
10.95	5o	C5n.2n (o)	70.356	−77.813	9.481	1.75	2.52	.662	3.49	2.72	3.92	10.6	8	31	47	7	4	3
12.29	5A	C5An.2n (m)	71.293	−76.115	10.631	1.25	.964	.497	1.45	1.12	1.60	3.84	8	29	52	10	5	3
13.06	5AA	C5AAn (m)	71.746	−75.122	11.283	1.37	1.55	.850	2.19	1.34	1.92	5.25	8	21	53	14	5	3
14.39	5AD	C5ADn (m)	72.381	−73.576	12.420	2.13	1.43	.702	1.60	1.11	1.55	3.61	8	22	54	14	5	3
15.09	5B	C5Bn.2n (m)	72.601	−73.192	13.012	2.78	4.48	1.92	4.50	2.97	4.15	9.77	8	24	53	14	6	3
16.15	5Cy	C5Cn.1n (m)	72.974	−72.498	13.948	2.27	6.11	3.17	7.43	4.10	5.52	16.3	8	18	53	17	5	3
16.64	5Co	C5Cn.3n (m)	73.181	−72.032	14.344	1.47	1.66	.802	2.28	1.21	1.75	5.33	8	18	51	17	5	3
17.47	5D	C5Dn (m)	73.394	−71.580	14.929	1.47	1.47	.678	1.72	1.04	1.47	3.97	8	17	52	18	5	3
18.28	5E	C5En (y)	73.617	−70.909	15.418	1.88	3.33	1.92	3.18	1.90	2.40	4.94	8	12	52	15	4	3
19.05	6y	C6n (y)	73.712	−70.936	15.946	1.41	2.02	.876	2.31	1.18	1.65	4.44	8	13	50	21	5	3
20.13	6o	C6n (o)	74.001	−70.157	16.727	1.93	2.00	.848	2.37	1.13	1.54	4.65	8	10	51	16	4	3
21.16	6A	C6An.2n (m)	74.133	−70.089	17.381	2.66	1.68	.796	2.09	1.14	1.58	4.36	8	12	52	11	4	3
23.07	6B	C6Bn.2n (o)	74.385	−69.727	18.675	2.83	3.51	1.83	4.07	1.95	1.71	9.31	8	10	55	16	4	3
24.06	6C	C6Cn.3n (m)	74.482	−69.581	19.347	2.08	2.33	1.21	2.56	1.36	1.77	4.59	8	9	55	11	3	3
24.84	7	C7n.2n (y)	74.509	−69.664	19.923	2.45	3.89	1.35	6.05	1.82	.416	1.86	8	9	56	18	4	3
25.82	8y	C8n.1n (y)	74.499	−69.836	20.625	2.03	4.18	2.23	4.20	2.04	2.35	6.79	8	12	59	9	3	3
26.55	8o	C8n.2n (o)	74.511	−69.806	21.175	1.12	2.73	1.51	3.01	1.63	2.13	5.22	8	15	60	12	4	3
27.03	9y	C9n (y)	74.455	−69.900	21.531	1.30	2.75	1.54	3.04	1.64	2.03	5.38	8	11	58	11	4	3
27.97	9o	C9n (o)	74.401	−69.747	22.234	1.30	2.42	1.44	2.63	1.57	2.08	4.34	8	14	60	17	4	3
28.28	10y	C10n.1n (y)	74.407	−69.504	22.575	1.58	2.13	1.32	2.28	1.51	2.03	3.88	8	17	59	17	5	3
28.75	10o	C10n.2n (o)	74.330	−69.543	22.953	2.92	2.33	1.32	2.48	1.36	1.77	3.95	8	13	67	17	5	3
29.40	11y	C11n.1n (y)	74.378	−68.714	23.662	2.20	1.81	1.09	2.14	1.42	1.91	4.16	8	18	57	21	6	3
30.10	11o	C11n.2n (o)	74.329	−68.430	24.232	1.12	1.94	.960	2.34	1.25	1.67	4.75	8	16	56	20	6	3
30.48	12y	C12n (y)	74.366	−67.750	24.708	2.67	1.97	1.00	2.10	1.30	1.74	3.88	8	16	48	18	5	3
30.94	12o	C12n (o)	74.320	−67.593	25.058	1.15	1.92	1.00	1.99	1.30	1.74	3.95	8	17	46	16	5	3
33.06	13y	C13n (y)	74.444	−64.739	26.969	1.83	3.27	1.67	3.13	1.63	2.17	4.92	8	16	45	23	7	3
33.55	13o	C13n (o)	74.479	−64.015	27.395	1.57	5.29	3.16	.72	2.68	3.37	6.19	8	15	49	21	6	3
34.66	15y	C15n (y)	74.621	−61.886	28.395	1.11	4.21	2.70	4.19	2.47	3.27	5.61	8	18	56	20	6	3
34.94	15o	C15n (o)	74.634	−61.485	28.615	2.77	1.22	.805	1.21	738	956	1.64	7	14	57	17	4	3
35.69	16y	C16n.2n (y)	74.702	−60.180	29.234	1.46	4.22	2.73	4.36	2.54	3.22	6.03	8	10	60	12	3	3
36.34	16o	C16n.2n (o)	74.750	−59.047	29.808	2.96	1.27	.852	1.30	.801	1.03	1.80	7	11	59	13	3	3
36.62	17y	C17n.1n (y)	74.763	−58.638	30.049	1.15	4.14	2.73	4.31	2.55	3.36	5.90	8	14	60	16	4	3
37.47	17o	C17n.1n (o)	74.816	−57.440	30.678	2.01	1.32	.885	1.37	.825	1.08	1.89	7	14	58	16	4	3
38.43	18y	C18n.1n (y)	74.855	−56.211	31.411	2.13	4.11	3.04	4.83	3.05	4.02	7.09	8	11	70	15	4	4
40.13	18o	C18n.2n (o)	74.868	−54.460	32.620	2.77	1.48	1.04	1.61	.982	1.34	2.24	7	16	58	21	6	4
41.39	19	C19n (m)	74.859	−53.254	33.532	1.01	4.91	2.75	5.98	2.72	4.00	9.71	8	15	49	17	7	4
42.54	20y	C20n (y)	74.856	−52.225	34.217	1.85	3.21	1.60	3.94	1.48	1.94	6.15	7	16	30	16	6	3
43.79	20o	C20n (o)	74.775	−51.610	35.288	1.06	5.71	.227	8.84	.258	.295	14.6	7	8	14	10	3	1

[a] Ages are from *Cande and Kent* [1995] except for chrons C3Ay and C3Ao, which are from *Krijgsman et al.* [1999]. Mag. An., magnetic anomaly; (y), (o), and (m), young and old ends and middle of Polarity Chron, respectively. Mag. Pts, FZ Pts, and Ab. hill Pts, the number of magnetic anomaly, fracture zone, and abyssal hill points, respectively. Mag. Segs and FZ Segs, the number of segments with magnetic anomaly and fracture zone data, respectively. The covariance matrix is given by the formula $\frac{1}{\hat{\kappa}} * \begin{pmatrix} a & b & c \\ b & d & e \\ c & e & f \end{pmatrix} * 10^{-g}$, where the values of a-f are given in radians squared.

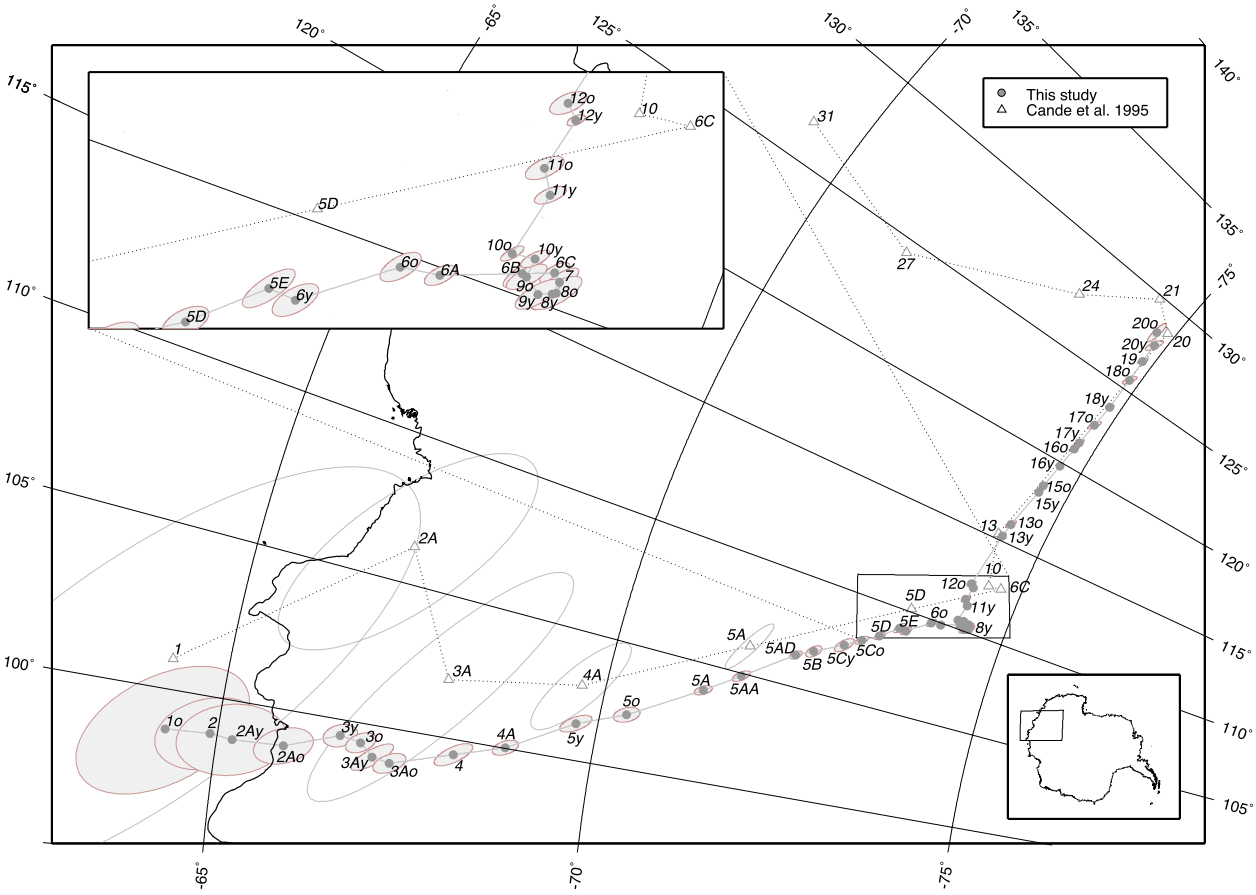

Figure 6. Comparison of our rotation poles (solid line) with the *Cande et al.* [1995] poles (dashed line) for the Pacific-Antarctic Ridge. Shaded ellipses show 95% confidence regions associated with the new poles. Open ellipses represent 95% confidence regions for chron C5A (12.3 Ma) and younger from *Cande et al.* [1995]. All poles are antipodal to those listed in Table 1. Map projection is stereographic centered on 69°S, 180°W.

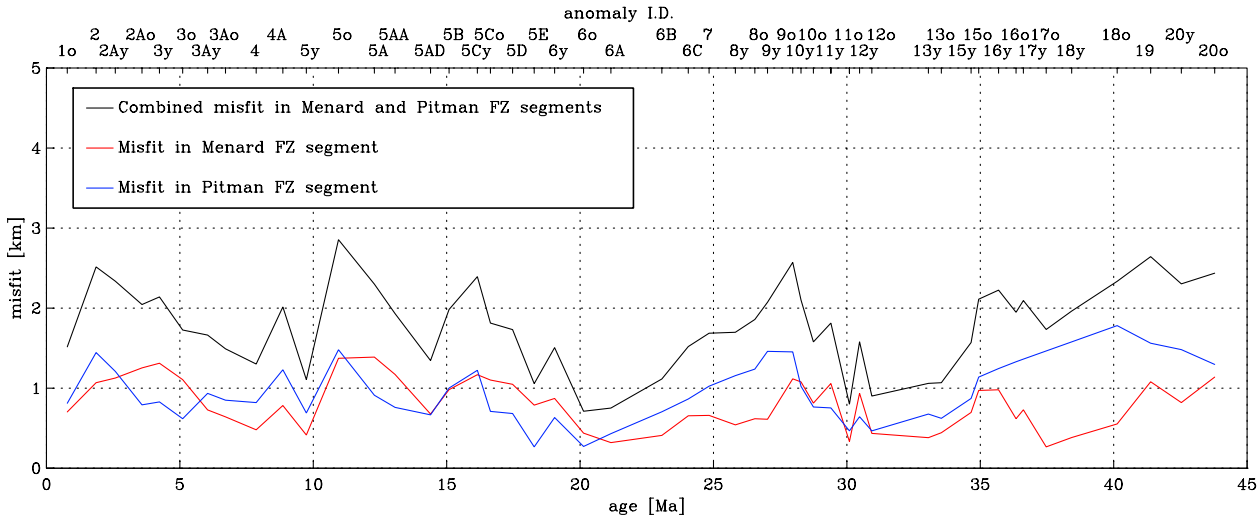

Figure 7. Individual and combined misfit in the Menard and Pitman FZ segments according to the *Chang* [1987, 1988] method.

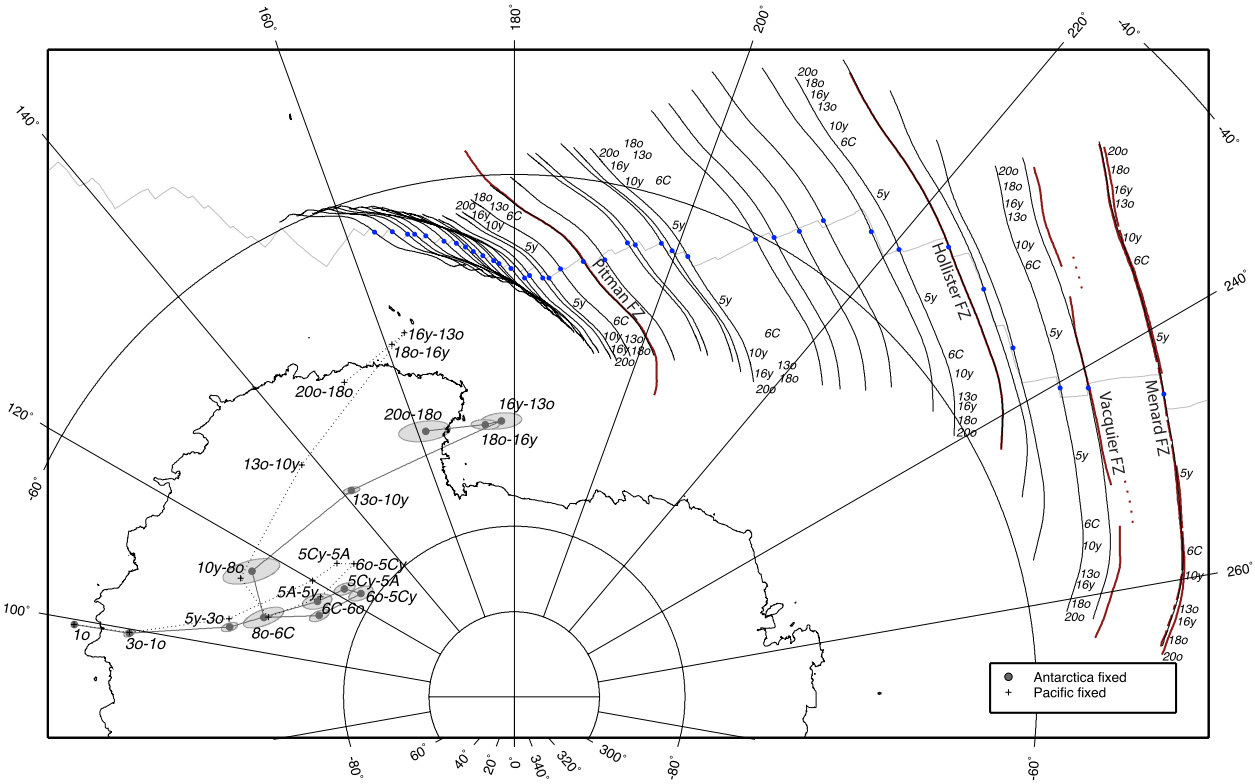

Figure 8. Stage poles for Pacific-Antarctic relative displacements. Gray dots and crosses are poles in the Antarctic plate and Pacific plate reference frames, respectively. Synthetic flow lines (black) based on the poles are plotted for many of the present-day ridge offsets. Blue dots mark the center points of the flow lines. The traces of the Menard, Vacquier, Hollister, and Pitman FZs are highlighted in red. The 95% confidence regions are shown for the stage poles in the Antarctic reference frame. Pacific-fixed 95% confidence regions are similar in size but are omitted for clarity. Map projection same as in Figure 6.

C5A (12.3 Ma) just north of the Menard FZ. Our new data show that since chron C5Cy half-spreading rates increased from 36 to about 43 mm/a at chron C3o (5.1 Ma) and remained constant from then until present.

[13] Large fluctuations in spreading rate of short durations (e.g., between chrons C17y and C15y) are probably not real but a result of small errors in magnetic anomaly picks, which are reflected in a larger error in the spreading rate calculation for short time intervals of about 1 Ma. In Figure 9 we excluded some of the 49 new rotations for chrons spaced at time intervals on the order of 0.5 Ma in order to smooth unrealistically large fluctuations. Small fluctuations in spreading rate, such as those between chrons C5Cy and C5o, may reflect small errors in magnetic anomaly picks or errors in the timescale. In order to evaluate the effect of timescale error we also looked at the Geologic Time Scale (GTS2004, red line on Figure 9) [*Ogg and Smith*, 2004], which includes the astronomically tuned timescale for the Neogene [*Lourens et al.*, 2004]. We found that spreading rate fluctuations are still present. The GTS2004 timescale leads to larger spreading rate fluctuations than the CK95 timescale for the PAR between chrons C5Cy and C4 (16.2 and 7.9 Ma), while the opposite is true between chrons C6B and C5Cy (23.1 and 16.2 Ma for CK95). However, these fluctuations in spreading rate over short time intervals are similar to the magnitude of the 95% confidence limits based on stage rotations (Figure 9).

[14] We used half-spreading rates based on the synthetic flow line to compute age versus distance, and compared these to observations from R/VIB *Nathaniel B. Palmer* cruise NBP9707. This cruise followed a track perpendicular to spreading lineation azimuths just north of Menard FZ and has a continuous magnetic anomaly record until chron C18o (40.1 Ma) on both the Pacific and Antarctic plates. The observed and predicted distances (Figure 10) show a good correlation, which is

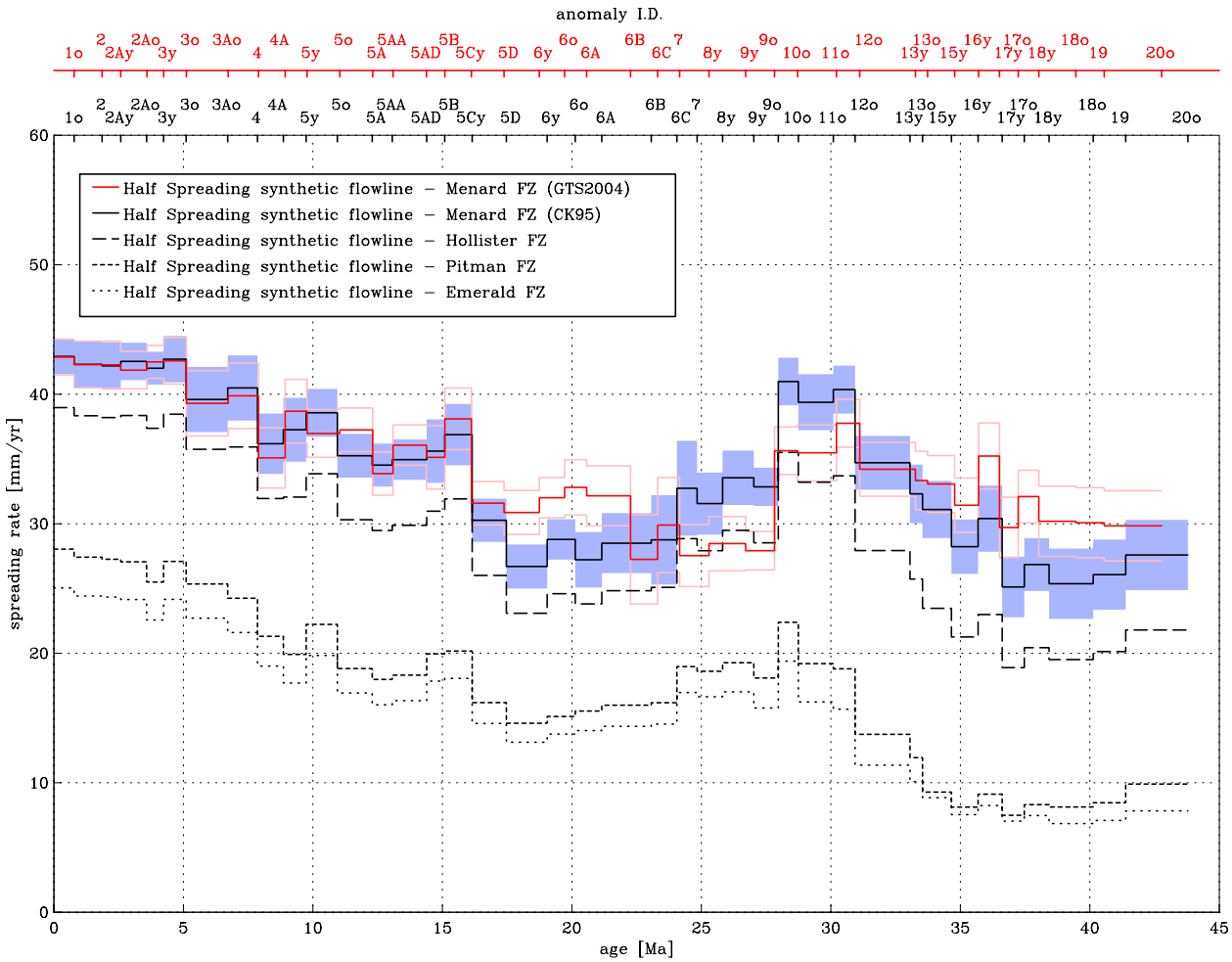

Figure 9. Half-spreading rates calculated from the rotation parameters along flow lines at the Menard, Hollister, Pitman, and Emerald FZs. Black lines represent spreading rates based on the CK95 timescale [*Cande and Kent*, 1995], and the red line represents spreading rates based on the GTS2004 timescale [*Ogg and Smith*, 2004]. Shading and pink lines are the 95% confidence limits based on stage rotations for the CK95 and GTS2004 timescales, respectively.

expected since the NBP9707 data were used in the calculation of the rotation parameters. Since chron C18o a total of 1460 km of Antarctic and 1350 km of Pacific oceanic crust has been accreted north of the Menard FZ. Apparently the PAR at this latitude has spread slightly asymmetrically since 40 Ma with more material accreted to the Antarctic plate.

6. Reconstruction of the Menard FZ

[15] The spreading ridge adjacent to the Menard FZ accreted almost 3000 km of oceanic crust since chron C20o (43.8 Ma). Seafloor depths range from about 2300 m at the axis (Figure 4c) to 5200 m at the oldest parts of the ocean floor near the FZ (Figures 4a and 4e). The ridge exhibits a smooth triangular morphology with an axial high [*Klingelhoefer et al.*, 2006; *Macdonald et al.*, 1988]. Troughs as deep as 6500 m mark the intersection of the FZ with the Henry and Hudson Troughs on the Pacific and Antarctic plates, respectively [*Eakins*, 2002; *Cande et al.*, 1982].

[16] The Menard FZ experienced adaptations to changes in plate motion. At its start, the FZ consisted of two splays, 30 km apart. Figure 11 shows the lineation azimuths based on the synthetic flow line and the ridge offset calculated from magnetic anomaly points across the Menard FZ during the last 40 Ma for both the Pacific and Antarctic plates. The ridge offsets on the two flanks should be the same; small differences reflect the uncertainties in the magnetic anomaly picks.

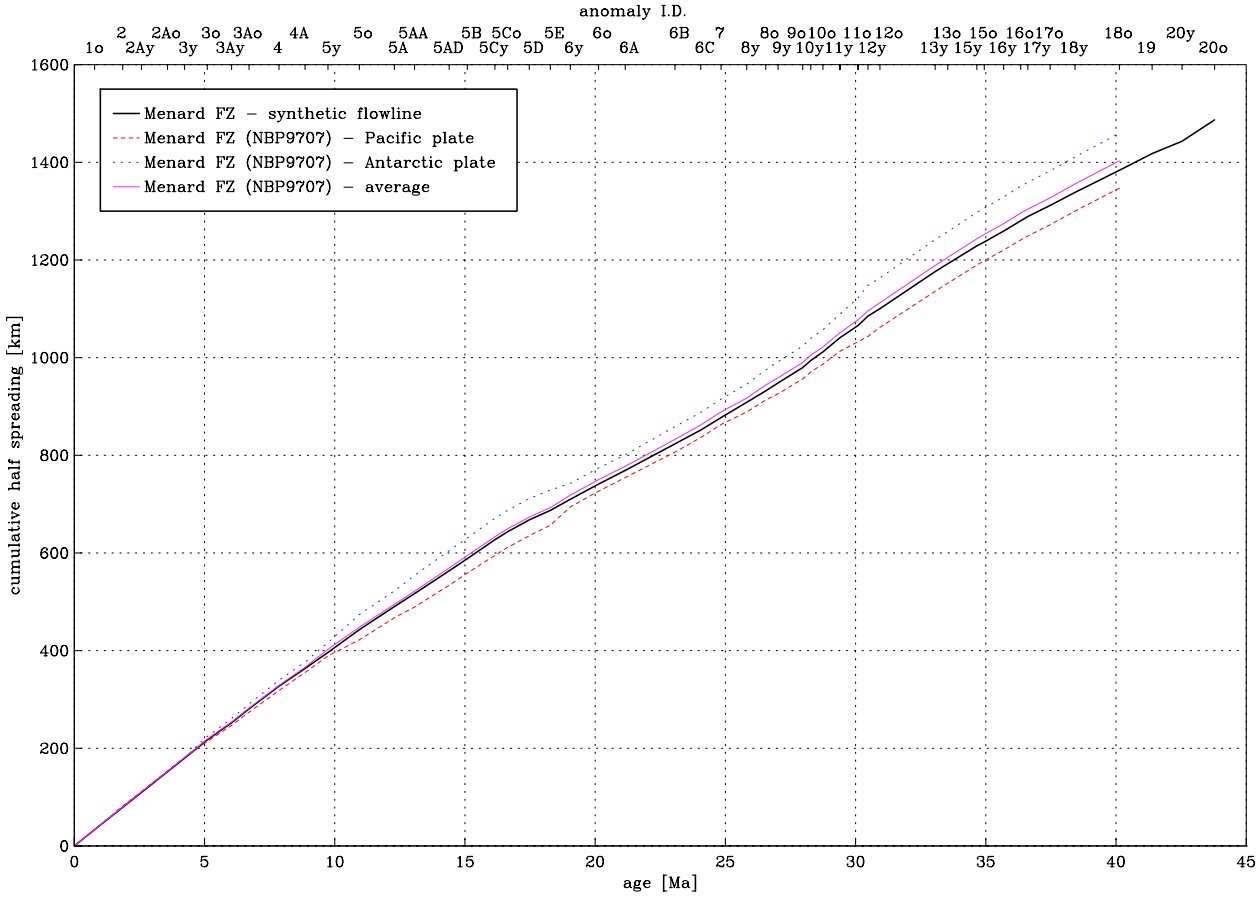

Figure 10. Cumulative half-spreading based on the flow line at the Menard FZ in comparison with the NBP9707 ship track that followed a route perpendicular to spreading lineation azimuths about 100 km north of the FZ.

The eastward drift of the stage poles between chrons C18o and C16y (40.1 to 35.7 Ma) put the FZ slightly under extension and the distance separating the two splays grew to about 35 km. During this period the ridge offset decreased from 150 to 130 km, corresponding to a 2° clockwise change in lineation azimuths. On the Pacific plate parallel to the northern splay at −46.2°S and 229.8°E (Figure 4a) a ridge rises 1200 m above the seafloor. This ridge possibly formed by transtension during the rotation. However, no prominent ridges are observed at the southern splay on the Pacific plate or at the conjugate splays on the Antarctic plate (Figure 4e). Note that there is a gap in multibeam bathymetry data on the location of much of the southern splay (Figure 4e). Ridges that rise up to 500 m above the surrounding seafloor are observed along most of the FZ splays. This relief can be explained by differential cooling and flexure of the rise flanks [*Sandwell*, 1984]. South of the Menard FZ no ridge offset data are available between 27 and 24 Ma owing to a ridge jump, which is possibly related to a propagating ridge around chron C7 (24.8 Ma). The westward ridge jump (Figure 4a) transferred about 65 km of former Pacific oceanic crust to the Antarctic plate (Figure 4d), which increased the ridge offset to about 230 km. A bathymetric deep of 800 m below the surrounding oceanic crust (Figure 4a) reveals the topographic scar of this jump on the Pacific plate. Chaotic magnetic anomalies and large changes in relief up to 1000 m characterize the captured former Pacific oceanic crust on the Antarctic plate south of the southern splay (Figure 4d).

[17] Between chrons C13o and C6C (33.5 to 24.1 Ma) the stage poles drifted westward, away from the plate boundary, with respect to both plates, which put the FZ under compression. Lineation azimuths experienced a counterclockwise change of about 15° and the corridor between the two splays gradually narrowed to a width of 5 to 10 km by chron C6C (23.1 Ma). The counterclockwise rotation is consistent with observations of *Cande et al.* [1995] and *Lonsdale* [1994a] for the northern part of the PAR; our study shows that this reorientation

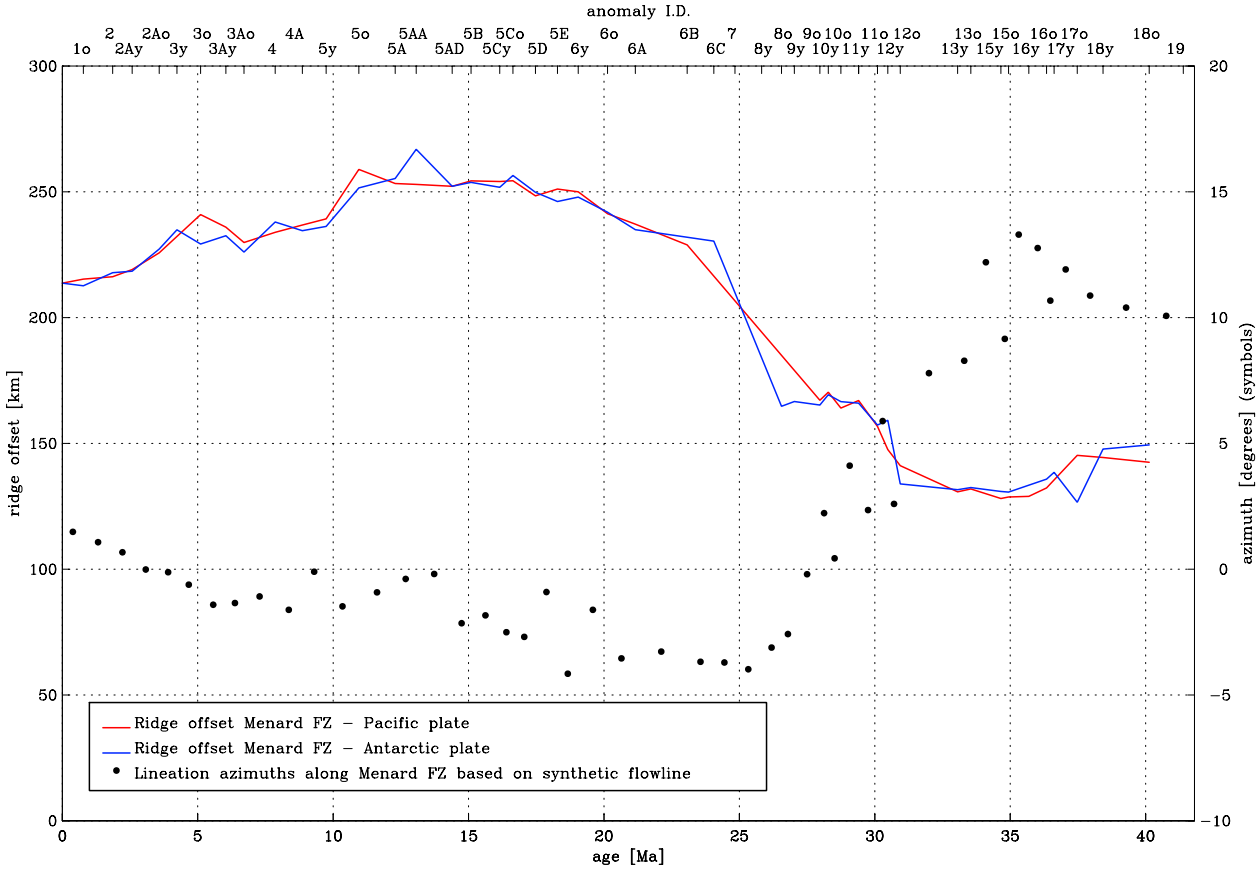

Figure 11. Ridge offset (lines) and lineation azimuths (dots) calculated from the rotation parameters at the Menard FZ. Oblique Mercator projection used to calculate lineation azimuths same as in Figures 1, 2, 3, and 5.

occurred progressively between 34 and 26 Ma. Between 24 and 11 Ma the ridge offset increased gradually from 230 to 260 km. This slight increase in transform fault offset at the right-stepping Menard FZ could indicate transpression. However, the spreading direction of the ridge segments near the Menard FZ remained fairly constant between chrons C6C and C3o (23.1 to 5.1 Ma) with only a 3° clockwise rotation as opposed to the Pitman and Emerald FZs [*Cande et al.*, 1995], which lie closer to the stage poles and underwent significant clockwise rotations since 10 Ma. During this period the ridge offset of Menard FZ gradually decreased to its modern value of 215 km. A 3° clockwise rotation since chron C3o (5.1 Ma) indicates the Menard transform fault is under transtension. At 4.9 Ma, after a remarkable 18 Ma lifespan of the narrow corridor, the northern splay of the Menard FZ ceased to exist leaving a single transform fault. The extensional period since chron C3o is reflected in a 5500 m deep Menard transform fault graben (Figure 4c) bounded by a transverse ridge on the north side that rises up to 2500 m below sealevel (Figure 4c). Moreover, a seamount peaks 2500 m below sea surface in the middle of the graben. A possible explanation for this feature is a leaky transform fault as envisioned by *Menard and Atwater* [1969] and *Menard and Chase* [1970].

7. Reconstruction of the Emerald FZ

[18] The southwestern section of the PAR, between the Terror FZ and the Macquarie Triple Junction, which links the Pacific, Antarctic and Australian plates, is located close to the rotation poles. This area has alternated periods of motion along a large transform fault with periods of spreading. Its complex tectonic history is therefore useful to test the predictive quality of the new rotation parameters. At present the area is characterized by multiple NNW-SSE striking en echelon faults and short spreading links. *Menard and Atwater* [1969] described how an opening of a transform fault in response to a change in plate motion creates an array of en echelon faults with the new spreading-

parallel azimuth and short linking spreading axes between them. Multiple en echelon faults and short spreading links were also considered for the Valdivia FZ System during the Neogene at the Antarctic-Nazca boundary [*Tebbens and Cande*, 1997; *Tebbens et al.*, 1997], for the Molokai and Mendocino-Pau-Pioneer systems during the late Cretaceous [*Atwater et al.*, 1993; *Searle et al.*, 1993] in the North Pacific and for the Andrew Bain FZ area during the late Cretaceous [*Royer et al.*, 1988; *Bernard et al.*, 2005] at the Southwest Indian Ridge.

[19] We reconstructed the evolution of the Emerald FZ on the basis of the synthetic flow lines with the Antarctic plate kept fixed. Figure 12 shows the evolution of the PAR close to the Macquarie Triple Junction since chron C24o (53.3 Ma). The major plate reorganization at ~45 Ma resulted in a 30° counterclockwise change in spreading direction. As a response, a transform fault of about 450 km offset formed between the Macquarie Triple Junction and the Emerald, E and Terror FZs (Figure 12: 43.8 Ma). Between chrons C20o and C13o (43.8 to 33.5 Ma) the transform fault lengthened to about 700 km. Around chron C13o a gradual 20° clockwise change in spreading direction put the transform fault under extension. The change in direction was small and it is not clear if distinct transform faults and ridges formed. A gradual 20° counterclockwise change in spreading direction starting around chron C10y (28.3 Ma) led once more to the formation of a single long transform fault between the Macquarie Triple Junction and Terror FZ by chron C6C (Figure 12: 24.1 Ma). The transform fault grew to a length of about 1200 km between chrons C6C and C5y (24.1 to 9.7 Ma). *Symons et al.* [2004] considered a leaky transform fault between 26.6 and 10.9 Ma accommodating some divergence between the Pacific and Antarctic plates and evolution of the transform fault into a spreading ridge since 5.9 Ma. Our observations suggest that there was pure transform motion during most of this period.

[20] Since chron C5y (9.7 Ma) the southwestern section of the PAR was subject to almost 30° of clockwise change in spreading direction. The change in spreading direction, starting around chron C5y, is associated with the northward migration of stage poles since that time, which put the long transform fault under extension and replaced it with an array of 15 transform faults and short ridge segments (Figure 12 for 9.7, 6.7 and 3.6 Ma and Figure 5 for 0 Ma). Ridges that run parallel to the original locations of the transform fault were most likely formed as flexural responses to the extension and related opening of the transform fault around chrons C13o and C5y (33.5 and 9.8 Ma). Similar extensional ridges are observed along the Udintsev FZ [*Lonsdale*, 1986, 1994b].

8. Effects Elsewhere on the PAR

[21] The effects of the clockwise change in spreading direction starting around chron C5y (9.7 Ma) associated with the northward migration of the stage poles since that time, continued with the increase in spreading rate around chron C4 (7.9 Ma) and are observed elsewhere on the PAR. South of the Heirtzler FZ this recent change in plate motion led to the formation of a short right-stepping ridge offset around chron C3Ay (6.0 Ma) and propagating rifts around chrons C2Ay and C1o (2.6 and 0.78 Ma) [*Briais et al.*, 2002]. The pattern of en echelon right-stepping faults and short spreading segments for Heezen, Udintsev and Raitt transform faults and the exceptional 6000 m depth of the Heezen and Tharp transform fault valleys, which are part of the Eltanin Fault System, have also been

Figure 12. Reconstruction of the Emerald, Terror, Erebus, and Kohiku FZs and FZs A through O (red flow lines and tags) based on the rotation parameters in Table 1. Antarctic plate is fixed. Frames show configurations at 3.6 Ma (chron C2Ao), 6.7 Ma (chron C3Ao), 9.7 Ma (chron C5y), 24.1 Ma (chron C6C), 33.1 Ma (chron C13o), 43.8 Ma (chron C20o) and 53.3 Ma (chron C24o). Blue dots mark the center points of the flow lines. The black tagged lines are isochrons based on magnetic anomaly picks, and the location of paleo-spreading ridges is highlighted with thick red lines. Dark blue lines mark the edges of the array of FZs A through O, and the bounding transverse ridges are contoured light blue. Colors represent the seafloor spreading provinces: blue and purple regions were generated by Pacific-Antarctic spreading, the yellow and light green regions were generated by Australia-East Antarctic spreading, the yellowish brown and green regions were generated by Australia-Antarctic spreading before chron C8 (26.6 Ma), the dark green and orange regions were generated by Australia-Lord Howe Rise (Tasman Sea) spreading, and the pink region was generated by Australia-Pacific spreading between chrons C20 and C8 (43.8 to 26.6 Ma). The Iselin Rift, an extensional plate boundary between West and East Antarctica prior to chron C24 (53.3 Ma) [*Marks and Stock*, 1997], is shown as a dark gray dashed line. Map projection same as in Figures 1, 2, 3, and 5. See Figure 5 for the present configuration of these transform faults.

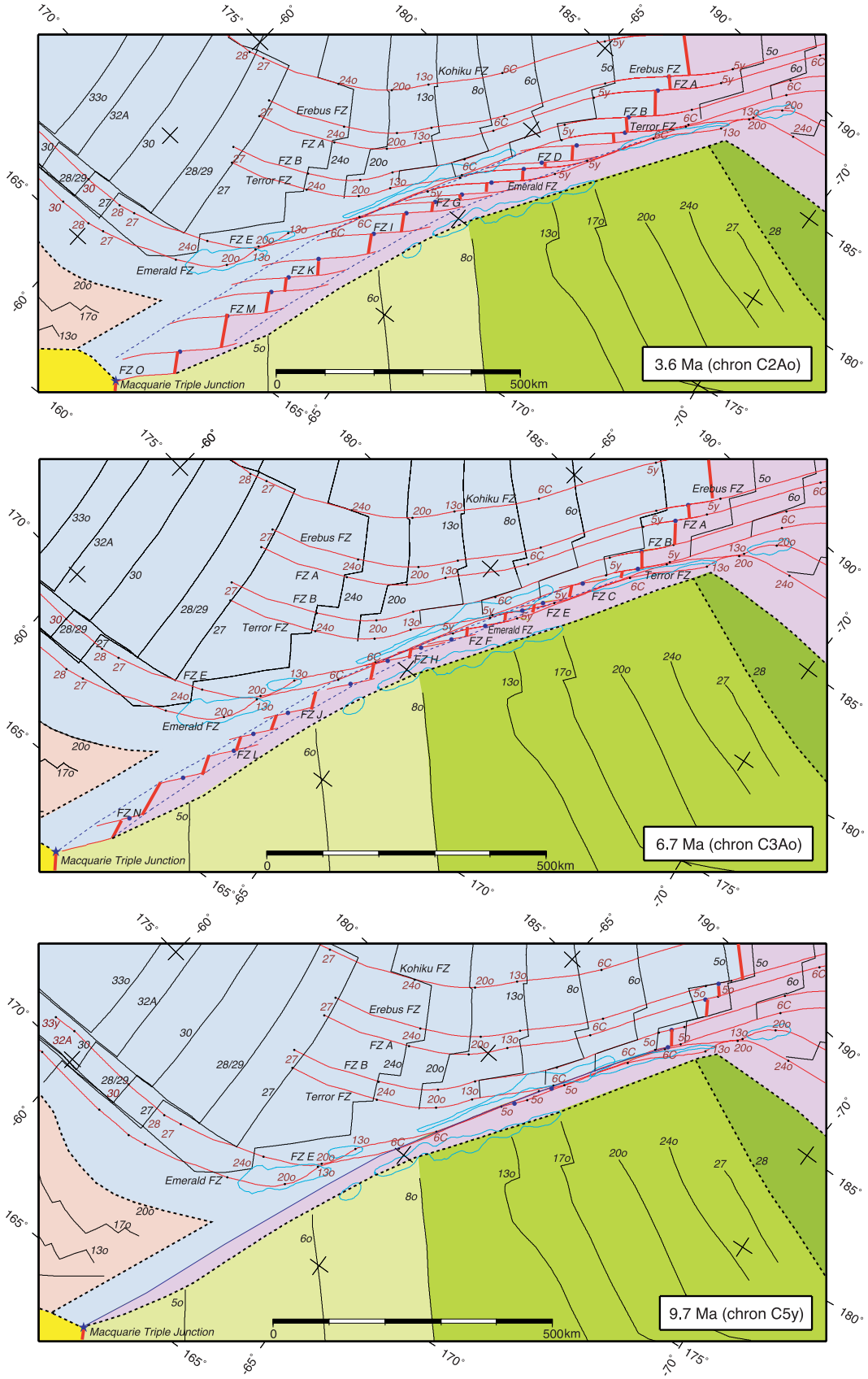
Kohiku FZ
Erebus FZ
FZ A
FZ B
Terror FZ
FZ C
FZ D
Emerald FZ
FZ E
FZ F
FZ G
FZ H
FZ I
FZ J
FZ K
FZ L
FZ M
FZ N
FZ O
Macquarie Triple Junction
0
500km
3.6 Ma (chron C2Ao)
6.7 Ma (chron C3Ao)
9.7 Ma (chron C5y)

Figure 12

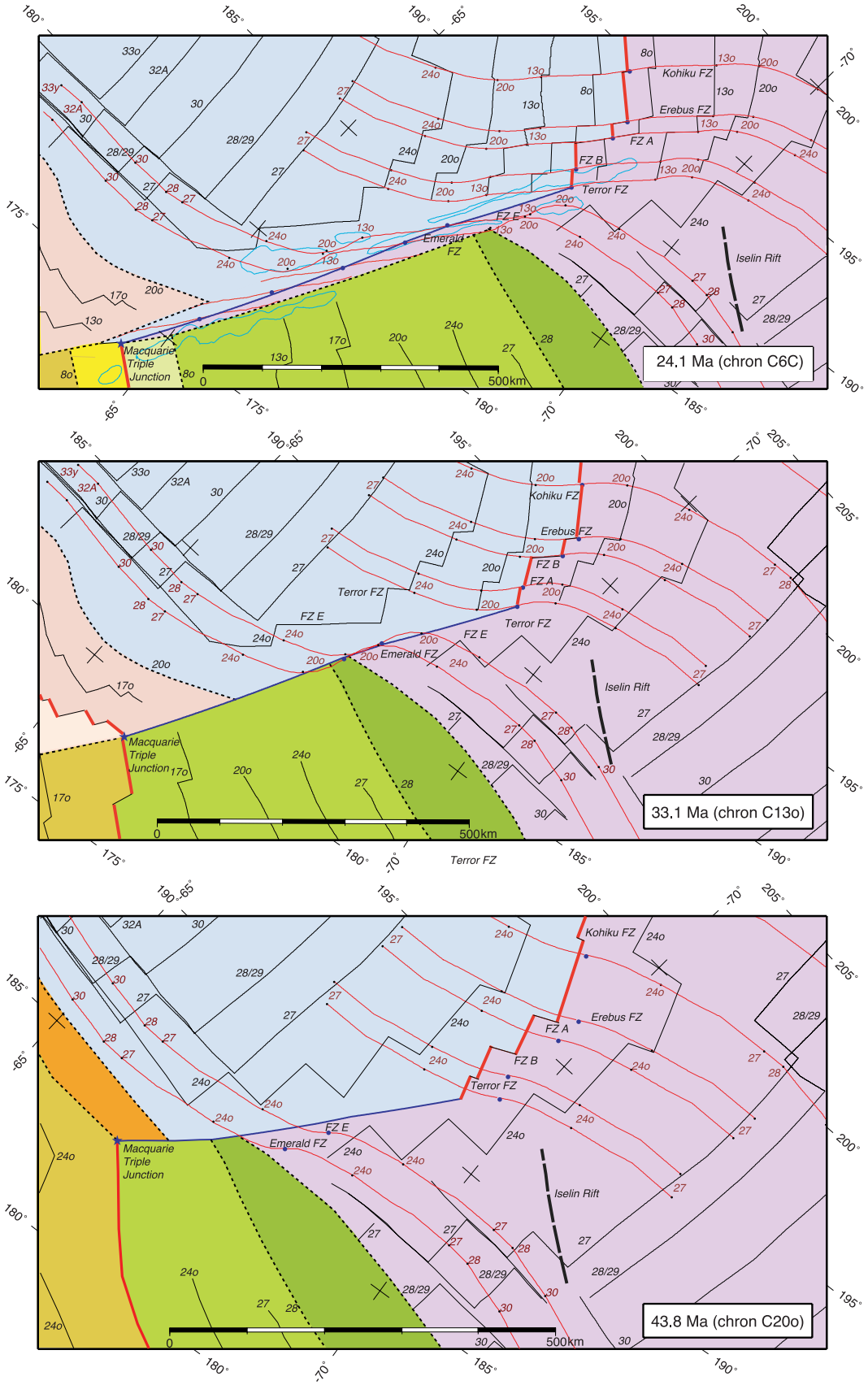

Figure 12. (continued)

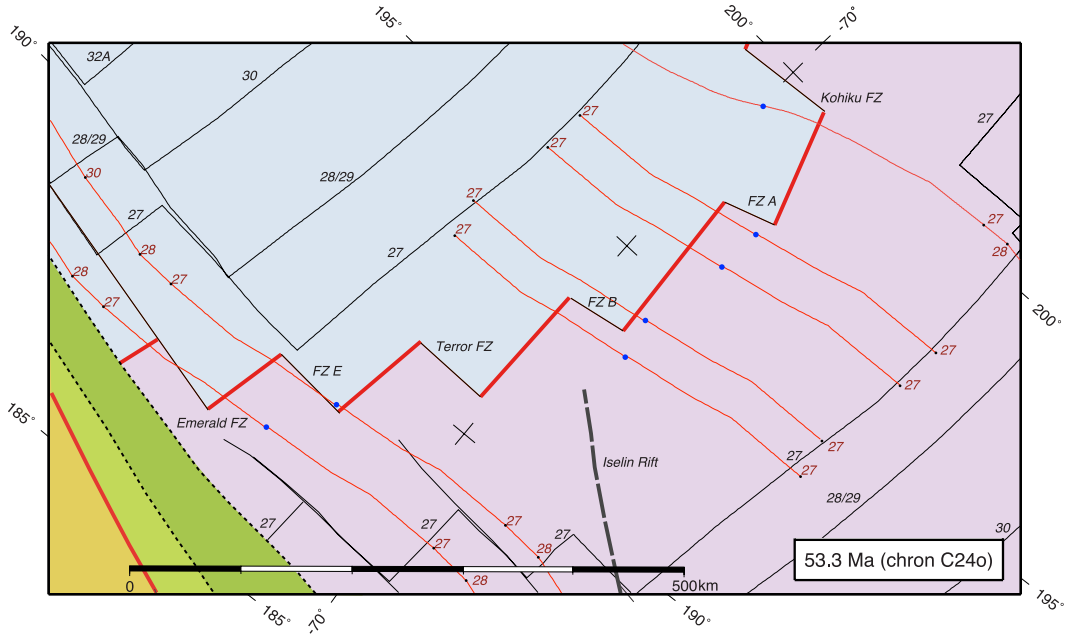

Figure 12. (continued)

attributed to extension resulting from the clockwise change in spreading direction during the Pliocene [*Lonsdale*, 1986, 1994b].

9. Global Tectonics

[22] *Atwater and Molnar* [1973] and *Stock and Molnar* [1988] pointed out the importance of the reconstruction of the PAR for motion of the Pacific plate relative to western North America. The rotation parameters based on the Pitman FZ [*Cande et al.*, 1995] were used by *Royer et al.* [2006] to revise the North America - Nubia - Antarctica - Pacific - North America plate circuit. Our Pacific-Antarctic rotation parameters are slightly different than the Pacific-Antarctic component of the plate circuit published by *Royer et al.* [2006], whose study focused on the effect of significantly modifying rotation parameters for the Southwest Indian Ridge. The effect of using our revised Pacific-Antarctic rotations is small compared to the effect of the significant changes in Southwest Indian Ridge rotation parameters proposed by *Royer et al.* [2006].

10. Summary and Conclusions

[23] In this study we determined 49 rotations that describe the relative motion between the Pacific and Antarctic plates since ~44 Ma in detail. We used data along the entire PAR, but the rotations were primarily constrained by the new detailed data set along the Menard FZ in combination with the Pitman FZ data. These two FZs are located ~3500 km apart and therefore cover a large area of PAR oceanic crust, allowing for tight constraints on rotation parameters. An outcome of this study is that our high-resolution plate motion model for the PAR can predict the plate tectonic history along the entire ridge in great detail. We tested the predictive quality of the stage rotations and synthetic flow lines based on these new rotation parameters at the southwestern end of the PAR close to the Macquarie Triple Junction. Reconstructions show that this section of the ridge twice became a single, long transform fault (between 44 and 33 Ma and between 24 and 10 Ma), followed by plate motion changes that put the transform fault into extension (between 33 and 28 Ma and from 10 Ma to present). During the most recent period of extension the transform fault was replaced by an array of 15 transform faults and short spreading centers. The earlier period of extension was not as long nor characterized by as large a change in direction and it is not clear if distinct transform faults and spreading ridges formed.

Acknowledgments

[24] This study was made possible through a series of grants from the NSF-Office of Polar Programs supporting the acquisition of geophysical data along transits of the R/VIB *Nathaniel B. Palmer*: grants OPP-0338317, OPP-0338346, OPP-

0126334, and OPP-0126340. We thank the officers, crew, and scientific staff of the R/VIB *Nathaniel B. Palmer* and the many students who sailed on these cruises. Caltech contribution 9005.

References

Atwater, T., and P. Molnar (1973), Relative motion of the Pacific and North American plates deduced from sea-floor spreading in the Atlantic, Indian and South Pacific Oceans, in *Proceedings of the Conference on Tectonic Problems of the San Andreas Fault*, *Stanford Univ. Publ. Geol. Sci.*, vol. 13, edited by R. L. Kovach and A. Nur, pp. 136–148, Stanford, Calif.

Atwater, T., and J. Severinghaus (1989), Tectonic maps of the northeast Pacific, in *The Geology of North America*, vol. N, *The Eastern Pacific Ocean and Hawaii*, edited by E. L. Winterer, D. M. Hussong, and R. W. Decker, pp. 15–20, Geol. Soc. of Am., Boulder, Colo.

Atwater, T., J. Sclater, D. Sandwell, J. Severinghaus, and M. S. Marlow (1993), Fracture zone traces across the North Pacific Cretaceous Quiet Zone and their tectonic implications, in *The Mesozoic Pacific: Geology, Tectonics, and Volcanism*, *Geophys. Monogr. Ser.*, vol. 77, edited by M. S. Pringle et al., pp. 137–154, AGU, Washington, D. C.

Bernard, A., M. Munschy, Y. Rotstein, and D. Sauter (2005), Refined spreading history at the Southwest Indian Ridge for the last 96 Ma, with the aid of satellite gravity data, *Geophys. J. Int.*, *162*(3), 765–778, doi:10.1111/j.1365-246X.2005.02672.x.

Briais, A., D. Aslanian, L. Géli, and H. Ondréas (2002), Analysis of propagators along the Pacific-Antarctic Ridge: Evidence for triggering by kinematic changes, Earth Planet, *Sci. Lett.*, *199*(3–4), 415–428, doi:10.1007/BF00286203.

Cande, S. C., and D. V. Kent (1995), Revised calibration of the geomagnetic polarity timescale for the Late Cretaceous and Cenozoic, *J. Geophys. Res.*, *100*(B4), 6093–6095, doi:10.1029/94JB03098.

Cande, S. C., and J. M. Stock (2004a), Pacific-Antarctic-Australia motion and the formation of the Macquarie Plate, *Geophys. J. Int.*, *157*(1), 399–414, doi:10.1111/j.1365-2699.2006.01643.x.

Cande, S. C., and J. M. Stock (2004b), Cenozoic reconstructions of the Australia-New Zealand-South Pacific Sector of Antarctica, in *The Cenozoic Southern Ocean: Tectonics, Sedimentation and Climate Change Between Australia and Antarctica*, *Geophys. Monogr. Ser.*, vol. 151, edited by N. Exxon, J. P. Kennett, and M. J. Malone, pp. 5–15, AGU, Washington, D. C.

Cande, S. C., E. M. Herron, and B. R. Hall (1982), The early Cenozoic tectonic history of the southeast Pacific, *Earth Planet. Sci. Lett.*, *57*(1), 63–74, doi:10.1016/0012-821X(82)90173-X.

Cande, S. C., J. L. LaBrecque, and W. F. Haxby (1988), Plate kinematics of the South Atlantic: Chron C34 to present, *J. Geophys. Res.*, *93*(B11), 13,479–13,492.

Cande, S. C., C. A. Raymond, J. Stock, and W. F. Haxby (1995), Geophysics of the Pitman Fracture Zone and Pacific-Antarctic plate motions during the Cenozoic, *Science*, *270*(5238), 947–953, doi:10.1126/science.270.5238.947.

Chang, T. (1987), On the statistical properties of estimated rotations, *J. Geophys. Res.*, *92*(B7), 6319–6329.

Chang, T. (1988), Estimating the relative rotations of two tectonic plates from boundary crossings, *JASA J. Am. Stat. Assoc.*, *83*(404), 1178–1183.

Cochran, J. R., and J. C. Sempéré (1997), The southeast Indian ridge between 88°E and 118°E: Gravity anomalies and crustal accretion at intermediate spreading rates, *J. Geophys. Res.*, *102*(B7), 15,463–15,487, doi:10.1029/97JB00511.

DeMets, C., R. G. Gordon, D. F. Argus, and S. Stein (1990), Current plate motions, *Geophys. J. Int.*, *101*(2), 425–478.

Eakins, B. W. (2002), Structure and development of oceanic rifted margins, Ph.D. thesis, Scripps Inst. of Oceanogr., La Jolla, Calif.

Gallo, D. G., P. J. Fox, and K. C. Macdonald (1986), A sea beam investigation of the Clipperton Transform Fault: The morphotectonic expression of a fast slipping transform boundary, *J. Geophys. Res.*, *91*(B3), 3455–3468.

Gans, K. D., D. S. Wilson, and K. C. Macdonald (2003), Pacific Plate gravity lineaments: Diffuse extension or thermal contraction?, *Geochem. Geophys. Geosyst.*, *4*(9), 1074, doi:10.1029/2002GC000465.

Géli, L., D. Aslanian, J. L. Olivet, I. Vlastelic, L. Dosso, H. Guillou, and H. Bougault (1998), Location of Louisville hotspot and origin of Hollister ridge: Geophysical constraints, *Earth Planet Sci. Lett.*, *164*(1–2), 31–40, doi:10.1016/S0012-821X(98)00217-9.

Goodwillie, A. M., and B. Parsons (1992), Placing bounds on lithospheric deformation in the central Pacific Ocean, *Earth Planet. Sci. Lett.*, *111*(1), 123–139, doi:10.1016/0012-821X(92)90174-T.

Gordon, R. G. (1998), The plate tectonic approximation: Plate nonrigidity, diffuse plate boundaries, and global plate reconstructions, Annu, *Rev. Earth Planet. Sci.*, *26*, 615–642, doi:10.1146/annurev.earth.26.1.615.

Hellinger, S. J. (1981), The uncertainties of finite rotations in plate tectonics, *J. Geophys. Res*, *86*(B10), 9312–9318.

Klingelhoefer, F., H. Ondréas, A. Briais, C. Hamelin, and L. Dosso (2006), New structural and geochemical observations from the Pacific-Antarctic Ridge between 52°45'S and 41°15'S, *Geophys. Res. Lett.*, *33*, L21312, doi:10.1029/2006GL027335.

Krijgsman, W., F. J. Hilgen, I. Raffi, F. J. Sierro, and D. S. Wilson (1999), Chronology, causes and progression of the Messinian salinity crisis, *Nature*, *400*(6745), 652–655, doi:10.1038/23231.

Lodolo, E., and F. Coren (1997), A Late Miocene plate boundary reorganization along the westernmost Pacific-Antarctic ridge, *Tectonophysics*, *274*(4), 295–305, doi:10.1016/S0040-1951(97)00005-X.

Lonsdale, P. (1986), Tectonic and magmatic ridges in the Eltanin fault system, South Pacific, *Marine Geophysical Researches*, *8*(3), 203–242, doi:10.1007/BF00305484.

Lonsdale, P. (1994a), Geomorphology and structural segmentation of the crest of the southern (Pacific-Antarctic) East Pacific Rise, *J. Geophys. Res.*, *99*(B3), 4683–4702.

Lonsdale, P. (1994b), Structural geomorphology of the Eltanin fault system and adjacent transform faults of the Pacific-Antarctic plate boundary, *Mar. Geophys. Res.*, *16*(2), 105–143, doi:10.1007/BF01224756.

Lourens, L. J., F. Hilgen, N. J. Shackleton, J. Laskar, and D. S. Wilson (2004), The Neogene period, in *A Geological Time Scale*, edited by F. M. Gradstein, J. G. Ogg, and A.G. Smith, pp. 409–440, Cambridge Univ. Press, Cambridge, U. K.

Macdonald, K. C., P. J. Fox, L. J. Perram, M. F. Eisen, R. M. Haymon, S. P. Miller, S. M. Carbotte, M. H. Cormier, and A. N. Shor (1988), A new view of the mid-ocean ridge from the behaviour of ridge-axis discontinuities, *Nature*, *335*(6187), 217–225, doi:10.1038/335217a0.

Marks, K. M., and J. M. Stock (1997), Early Tertiary gravity field reconstructions of the southwest Pacific, *Earth Planet*

Sci. Lett., *152*(1-4), 267–274, doi:10.1016/S0012-821X(97)00139-8.

McAdoo, D., and S. Laxon (1997), Antarctic tectonics: Constraints from an ERS-1 satellite marine gravity field, *Science*, *276*(5312), 556–560, doi:10.1126/science.276.5312.556.

Menard, H.W., and T. Atwater (1969), Origin of fracture zone topography, *Nature*, *222*(5198), 1037–1040, doi:10.1038/2221037a0.

Menard, H. W., and T. E. Chase (1970), Fracture zones, in *The Sea*, vol. 4, part 1, edited by A. E. Maxwell, pp. 421–444, Wiley Intersci., New York.

Molnar, P., T. Atwater, J. Mammerickx, and S. M. Smith (1975), Magnetic anomalies, bathymetry and the tectonic evolution of the South Pacific since the Late Cretaceous, *Geophys. J. R. Astron. Soc.*, *40*(3), 383–420, doi:10.1111/j.1365-246X.1975.tb04139.x.

Ogg, J. G., and A. G. Smith (2004), The geomagnetic polarity time scale, in *A Geological Time Scale*, edited by F. M. Gradstein, J. G. Ogg, and A. G. Smith, pp. 63–86, Cambridge Univ. Press, Cambridge, U. K.

Pitman, W. C., E. M. Herron, and J. R. Heirtzler (1968), Magnetic anomalies in Pacific and sea floor spreading, *J. Geophys. Res.*, *73*(6), 2069–2085, doi:10.1126/science.154.3753.1164.

Royer, J.Y., and T. Chang (1991), Evidence for relative motions between the Indian and Australian Plates during the last 20 m.y. from plate tectonic reconstructions: Implication for the deformation of the Indo-Australian plate, *J. Geophys. Res.*, *96*(B7), 11,779–11,802.

Royer, J. Y., P. Patriat, H. W. Bergh, and C. R. Scotese (1988), Evolution of the Southwest Indian Ridge from the Late Cretaceous (anomaly 34) to the Middle Eocene (anomaly 20), *Tectonophysics*, *155*(1–4), 235–260.

Royer, J. Y., R. G. Gordon, and B. C. Horner-Johnson (2006), Motion of Nubia relative to Antarctica since 11 Ma: Implications for Nubia-Somalia, Pacific-North America, and India-Eurasia motion, *Geology*, *34*(6), 501–504, doi:10.1046/j.1365-246X.2003.01917.x.

Sandwell, D. T. (1984), Thermomechanical evolution of oceanic fracture zones, *J. Geophys. Res.*, *89*(B13), 1401–1413.

Sandwell, D. T., and W. H. F. Smith (1997), Marine gravity anomaly from Geosat and ERS 1 satellite altimetry, *J. Geophys. Res.*, *102*(B5), 10,039–10,054, doi:10.1029/96JB03223.

Searle, R. C., R. T. Bird, R. I. Rusby, and D. F. Naar (1993), The development of 2 oceanic microplates — Easter and Juan-Fernandez microplates, East Pacific Rise, *J. Geol. Soc.*, *150*, 965–976, doi:10.1144/gsjgs.150.5.0965.

Stock, J., and P. Molnar (1988), Uncertainties and implications of the late Cretaceous and Tertiary position of North America relative to the Farallon, Kula, and Pacific plates, *Tectonics*, *7*(6), 1339–1384.

Symons, C. M., T. A. Meckel, S. Mosher, and M. F. Coffin (2004), Plate kinematic model and resulting evolution of oceanic transform fault tectonics adjacent to the Macquarie Triple Junction, SW Pacific, *Eos Trans. AGU*, *85*(47), Fall Meet. Suppl., Abstract T41A-1161.

Tebbens, S. F., and S. C. Cande (1997), Southeast Pacific tectonic evolution from early Oligocene to present, *J. Geophys. Res.*, *102*(B6), 12,061–12,084, doi:10.1029/96JB02582.

Tebbens, S. F., S. C. Cande, L. Kovacs, J. C. Parra, J. L. LaBrecque, and H. Vergara (1997), The Chile ridge: A tectonic framework, *J. Geophys. Res.*, *102*(B6), 12,035–12,059, doi:10.1029/96JB02581.

Weiland, C. M., and K. C. Macdonald (1996), Geophysical study of the East Pacific Rise 15°N–17°N: An unusually robust segment, *J. Geophys. Res.*, *101*(B9), 20,257–20,273.